Journal of Heat and Mass Transfer Research 5 (2018) 51-68

Semnan University

Journal of Heat and Mass Transfer Research

Journal homepage: http://jhmtr.journals.semnan.ac.ir

Characterization of unsteady double-diffusive mixed convection flow with soret and dufour effects in a square enclosure with top moving lid

Omid Ghaffarpasand*

Department of Physics, University of Isfahan, Isfahan 81746, Iran

PAPER INFO

History:

Submitted: 2015-08-10
Revised: 2017-01-17
Accepted: 2017-02-01

Keywords :

Double-diffusive convection;
Soret and Dufour effects;
Heat and mass transfer;
Conduction.

A B S T R A C T

The present study considers the numerical examination of an unsteady thermo-solutal mixed convection when the extra mass and heat diffusions, called as Soret and Dufour effects, were not neglected. The numerical simulations were performed in a lid-driven cavity, where the horizontal walls were kept in constant temperatures and concentrations. The vertical walls were well insulated. A finite volume method based on SIMPLE algorithm was utilized to solve the coupled governing equations. Numerical simulations are performed for wide combinations of Soret and Duofour coefficients and are given by streamlines, isotherms, isoconcentrations, fluid velocities, average Nusselt and Sherwood numbers. The influences of pertinent parameters on the various heat transfer modes, *i.e.* convective and conductive modes, as well as the total kinematic energy of the studied thermo-solutal system are also analyzed.

Results demonstrate that Soret and Dufour effects insignificantly influence the fluid flow and transport phenomena when flow is affected to some extent by the forced convection. It is also achieved that the extra heat diffusion, Dufour effect, affects heat transfer by creating thermal eddies especially when flow is dominated by the natural convection. Besides, the conductive mode of heat transfer is attenuated by Dufour coefficient.

DOI: 10.22075/jhmtr.2017.1503.1100

1. Introduction

The convection simultaneously driven by temperature and concentration gradients are often called either double-diffusive or thermo-solutal convection. Double-diffusive convection is an attractive subject due to its wide scientific applications such as oceanography, astrophysics, geology, biology and chemical processes [1]. This aspect of fluid dynamics has been gained considerable attentions from the both of theoretical and experimental researchers because of its importance and wide practical applications such as electronic device cooling, multi-shield structures used for nuclear reactors, float gas production, crystal growth, drying processes, chemical reactors, and many others [2-6]. Based on that, wide advanced models as well as research methods have been developed to better understand the physical phenomena in involved in double-diffusive convection. Among the literature published on this subject, Lee & Hyun [8], and Hyun & Lee [9], numerically studied the double-diffusive convection in a rectangular enclosure with aiding and opposing temperature and concentration gradients. Their solution was significantly satisfied the experimental results. Oztop & Dagatekin numerically investigated the steady mixed convection in a two-sided lid-driven enclosure [10]. Results elucidate that the heat

Corresponding Author: *O. Ghaffarpasand, Department of Physics, University of Isfahan, Isfahan 81746, Iran*
Email: o.ghaffarpasand@gmail.com

transfer enhances as Richardson number Ri value decreases. Al-Amiri et al., utilized numerical simulations to look through the steady double-diffusive convection in a square lid-driven cavity [11]. Results demonstrate that heat transfer enhances as the buoyancy ratio increases. Thermo-solutal convection with temperature and concentration gradients at the same time in a rectangular enclosure was studied by Qin et al, [12]. They used a high-order compact scheme in their study. Jena et al., researched on the transient process of buoyancy-opposed thermo-solutal convection of micropolar fluids [13]. Bhattacharya and Das also used numerical techniques to investigate the steady thermo-solutal natural convection flow inside a usual lid-driven cavity [14]. It has been shown that Rayleigh number is an important parameter in the heat transfer variation. Wang et al., performed regularized Lattice Boltzmann method (LBM) to study thermo-solutal convection in the vertical cavity [15]. It has been shown that heat and mass transfer are attenuated as the cavity aspect ratio enhances.

It is well known that the fluid flow is simultaneously affected by temperature and concentration gradients as well in the double-diffusive convection flow. In some cases, the extra thermal and mass diffusivity called Dufour and Soret effects, respectively, affect on the thermo-solutal flow characteristics to some extent. Soret effect is the extra mass diffusivity caused by the temperature gradient, while Dufour effect refers to the energy flux created by the concentration gradient. The Soret and Dufour effects are called SD-effects hereinafter for the sake of brevity. SD-effects are ignored in many cases due to their order of magnitude respect to the effects described by Fourier's and Fick's laws. Moreover, they have usually considered as the second-order phenomena. Nevertheless, in some engineering and industrial applications such as chemical reactors, solidification of binary alloys, groundwater pollutant migration, hydrology and geosciences, when temperature and concentration gradients are large enough, the SD-effects could not be ignored and should be taken into account to complete the accurate simulation. In those cases, the temperature and concentration equations become coupled with each other. Recently, some investigators have been conducted numerical and analytical studies to study double-diffusive convection when SD-effects were not neglected.

Malashetty & Gaikward studied numerically the influence of SD-effects on thermo-solutal convection in an unbounded vertically stratified system [16]. Rebai et al., investigate double-diffusive convection in a square cavity filled with binary fluid mixture using the both numerical and analytical methods [17]. Soret effect was just considered by them. Bhuvaneswari et al., performed numerical simulations to investigate mixed convection flow with just Soret effect in a regular two-sided lid-driven square enclosure [18]. They looked into the relation of the lid's movement direction and transport phenomena, and found that both of heat and mass transfer are attenuated if the walls move in the same directions. Actually, they did not consider the influence of Soret effect alone, because all of their numerical simulations performed at a constant Soret coefficient. Wang et al., used an unsteady numerical model to research on the influence of SD-effects on thermo-solutal convection in a horizontal rectangular enclosure [19]. Results show that heat and mass transfer increase as the aspect ratio decreases. Their simulations performed in a stable cavity with no moving lid(s) and so they did not study the effects of shear forces on the double-diffusive convection. Recently, Ren & Chen utilized the LBM to study double-diffusive convection in a vertical enclosure with SD-effects [20]. They found that the average Nusselt and Sherwood numbers were increased with increasing Rayleigh number, Prandtl number, Lewis number, Soret and Dufour coefficients. Kefayati also used the LBM to examine double-diffusive convection with SD-effects in an inclined porous cavity [21]. The results prove that heat and mass transfer are sensitive greatly to the inclination angle. Wang et al., utilized an accurate finite volume method based on SIMPLE algorithm to investigate numerically an oscillatory double-diffusive convection in a horizontal cavity with SD-effects [22]. They found that double-diffusive convection develops from steady state convection dominated to chaotic flow as buoyancy ratio increases.

In all of the above studies, a constant set of Soret and Dufour coefficients was assumed during the simulations. On the other hand, to the author's best knowledge, the effect of SD-effects on the various modes of heat transfer has not been analysed yet. To be more precise, the contribution of each modes of heat transfer and in particular, the influence of extra mass and heat diffusions on those contributions have not been studied yet. In addition, although the

kinetic energy is a key factor in the design and optimization of thermal systems, the influence of SD-effects on the total energy of the thermo-solutal systems has not been considered, yet. Based on the above story, the main purpose of the present study is to characterize the unsteady thermo-solutal convection with SD-effects in one hand, and analyse the influence of SD-effects on the various modes of heat transfer as well as the total energy of the system in the other hand.

2. Model Description

The physical model configuration which consists of a square enclosure with just top moving wall in its own plane at constant velocity U_0, is displayed in Fig. 1. The top and bottom walls are maintained isothermally at uniform temperatures T_l and T_h respectively, $T_h > T_l$. The opposite boundary conditions are assumed for concentration at top and bottom walls, when those are maintained at concentrations C_h and C_l correspondingly, $C_h > C_l$. The vertical walls are assumed adiabatic and impermeable. This illustration creates a gravitationally-unstable temperature and concentration gradients and results in a thermo-solutal/double-diffusive convection.

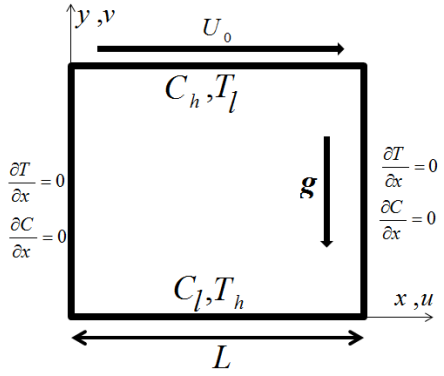

Fig. 1: Schematic diagram of the computational model.

The enclosure has an aspect ratio of unity ($A = 1$) and dry air is assumed as the working fluid, $Pr = 0.71$. Fluid is also assumed Newtonian and incompressible except for the density in the buoyancy term of the momentum equation in the vertical direction, according to the Bousinesq approximation. Accordingly, the density variation due to both temperature and concentration gradients can be written as:

$$\rho = \rho_0(1 - \beta_T(T - T_0) - \beta_C(C - C_0))$$

where $\beta_T = \frac{1}{\rho}(\frac{\partial \rho}{\partial T})_{(C,p)}$ and, $\beta_C = \frac{1}{\rho}(\frac{\partial \rho}{\partial T})_{(T,p)}$ are the thermal and concentration expansion coefficients, respectively. With these assumptions, the fundamental governing equations, including continuity, momentum, energy, and concentration (mass) equations can be expressed as:

$$\frac{\partial u}{\partial x} + \frac{\partial v}{\partial y} = 0 \quad (1)$$

$$\frac{\partial u}{\partial t} + u\frac{\partial u}{\partial x} + v\frac{\partial u}{\partial y} = -\frac{1}{\rho}\frac{\partial p}{\partial x} + \nu\left(\frac{\partial^2 u}{\partial x^2} + \frac{\partial^2 u}{\partial y^2}\right) \quad (2)$$

$$\frac{\partial v}{\partial t} + u\frac{\partial v}{\partial x} + v\frac{\partial v}{\partial y} = -\frac{1}{\rho}\frac{\partial p}{\partial y} + \nu\left(\frac{\partial^2 v}{\partial x^2} + \frac{\partial^2 v}{\partial y^2}\right) - \frac{\rho}{\rho_0}g \quad (3)$$

$$\frac{\partial T}{\partial t} + u\frac{\partial T}{\partial x} + v\frac{\partial T}{\partial y} = \alpha_m\left(\frac{\partial^2 T}{\partial x^2} + \frac{\partial^2 T}{\partial y^2}\right) + \kappa_{TC}\left(\frac{\partial^2 C}{\partial x^2} + \frac{\partial^2 C}{\partial y^2}\right) \quad (4)$$

$$\frac{\partial C}{\partial t} + u\frac{\partial C}{\partial x} + v\frac{\partial C}{\partial y} = D_m\left(\frac{\partial^2 C}{\partial x^2} + \frac{\partial^2 C}{\partial y^2}\right) + \kappa_{CT}\left(\frac{\partial^2 T}{\partial x^2} + \frac{\partial^2 T}{\partial y^2}\right) \quad (5)$$

where ν, g, α_m, D_m, κ_{TC}, κ_{CT} are kinematic viscosity, gravity acceleration, thermal diffusivity, diffusion coefficient, Soret and Dufour coefficients, respectively. The governing equations are then non-dimensionalized using the following dimensionless variables:

$$(X, Y) = \frac{(x, y)}{L}, (U, V) = \frac{(u, v)}{U_0}, P = \frac{p}{p_0}, \tau = \frac{t}{t_0}$$

$$\Theta = \frac{T - T_0}{T_h - T_l}, \quad \Phi = \frac{C - C_0}{C_h - C_l}$$

where t_0 is the characteristic time $t_0 = L/U$, p_0 is the characteristic pressure $p_0 = \rho U_0^2$, T_0 is the characteristic temperature, and C_0 is the characteristic particle concentration. Following Barletta & Zanchini [23], the characteristic temperature and concentration are assumed as $T_0 = (T_h + T_l)/2$ and $C_0 = (C_h + C_l)/2$, respectively. Therefore, the dimensionless form of governing equations are:

$$\frac{\partial U}{\partial X} + \frac{\partial V}{\partial Y} = 0 \quad (6)$$

$$\frac{\partial U}{\partial \tau}+U\frac{\partial U}{\partial X}+V\frac{\partial U}{\partial Y}=-\frac{\partial P}{\partial X}+\frac{1}{Re}\left(\frac{\partial^2 U}{\partial X^2}+\frac{\partial^2 U}{\partial Y^2}\right) \quad (7)$$

$$\frac{\partial V}{\partial \tau}+U\frac{\partial V}{\partial X}+V\frac{\partial V}{\partial Y}=-\frac{\partial P}{\partial Y}+\frac{1}{Re}\left(\frac{\partial^2 U}{\partial X^2}+\frac{\partial^2 V}{\partial Y^2}\right)+ Ri\left(\Theta+B\Phi\right) \quad (8)$$

$$\frac{\partial \Theta}{\partial \tau}+U\frac{\partial \Theta}{\partial X}+V\frac{\partial \Theta}{\partial Y}=\frac{1}{RePr}\left(\frac{\partial^2 \Theta}{\partial X^2}+\frac{\partial^2 \Theta}{\partial Y^2}\right)+ \frac{Df}{Re}\left(\frac{\partial^2 \Phi}{\partial X^2}+\frac{\partial^2 \Phi}{\partial Y^2}\right) \quad (9)$$

$$\frac{\partial \Phi}{\partial \tau}+U\frac{\partial \Phi}{\partial X}+V\frac{\partial \Phi}{\partial Y}=\frac{1}{ReSc}\left(\frac{\partial^2 \Phi}{\partial X^2}+\frac{\partial^2 \Phi}{\partial Y^2}\right)+ \frac{Sr}{Re}\left(\frac{\partial^2 \Theta}{\partial X^2}+\frac{\partial^2 \Theta}{\partial Y^2}\right) \quad (10)$$

The buoyancy ratio B, Lewis number Le, Richardson number Ri, Dufour coefficient Df, and Soret coefficient Sr, are defined as:

$$B=\frac{\beta_C (C_h-C_l)}{\beta_T (T_h-T_l)}=\frac{Gr_C}{Gr_T},\quad Le=\frac{Sc}{Pr},\quad Ri=\frac{Gr_T}{Re^2}$$

$$Df=\frac{\kappa_{TC} (C_h-C_l)}{\alpha_m (T_h-T_l)},\quad Sr=\frac{\kappa_{CT} (T_h-T_l)}{D_m (C_h-C_l)}$$

Richardson number value ususally illustrates the importance of natural convection relative to the forced convection, whereby the flow is dominated by forced and natural convction when $Ri \ll 1$ and $Ri \ll 1$, respectively. However, the boundary conditions in the dimensionless form are so:

$$X=0,1: U=V=0, \frac{\partial \Theta}{\partial X}=\frac{\partial \Phi}{\partial X}=0$$

$$Y=0: U=0, V=0, \Theta=1, \Phi=0$$

$$Y=1: U=+1, V=0, \Theta=0, \Phi=1$$

To examine the heat and mass transfer within the enclosure, the average Nusslet and Sherwood numbers on the horizontal walls with maximum temperature and concentration are examined. For this purpose, the local Nusselt and Sherwood numbers along the horizontal bottom and top walls, respectively, are defined as:

$$Nu(X)=-\left.\frac{\partial \Theta}{\partial Y}\right|_{Y=0}+Df\left.\frac{\partial \Phi}{\partial Y}\right|_{Y=0} \quad (11)$$

$$Sh(X)=-\left.\frac{\partial \Phi}{\partial Y}\right|_{Y=1}+Sr\left.\frac{\partial \Theta}{\partial Y}\right|_{Y=1} \quad (12)$$

The average Nusselt and Sherwood numbers then can be calculated as:

$$\overline{Nu}=\int_0^1 Nu(X)dX,\quad \overline{Sh}=\int_0^1 Sh(X)dX \quad (13)$$

It should be noted that the different boundary conditions are implied for temperature and concentration to better understand the influence of the extra available diffusions on the fluid characteristics and transport phenomena. To better understand and discuss the heat transport processes, the different modes of heat transfer, *i.e.* conductive and convective modes, across the enclosure are also examined by the relation proposed by Cheng [24]. For this purpose, Nusselt number along the vertical mid-plane of the enclosure is evaluated by the following equation:

$$Nu=\frac{\partial \Theta}{\partial Y}-\mathrm{Pr}.\mathrm{Re}.V.\Theta \quad (14)$$

where the first and second terms of this equation represent the contributions of heat transfer because of the conductive and convective modes, respectively. Further examination of the total kinetic energy is also implemented in this study. It is calculated using the expression proposed before by Goyan through [25]:

$$E=\sqrt{\sum_{(i,j)=(1,1)}^{(n_x,n_y)}\left[\left(U_{i,j}^2\right)+\left(V_{i,j}^2\right)\right]} \quad (15)$$

This equation is calculated on all of the grid nodes and averaged during final 1000 final time steps. The temporal variation of total kinetic energy is also analyzed in further to better examine the stationary state conditions.

3. Numerical Approach

The dimensionless governing equations, Eqs. (6)-(10), are firstly discretized on a staggered grid by a finite volume method developed by Patankar [26]. The convection terms are discretized using the *QUICK* scheme, while a second-order Adams-Bashforth explicit scheme is implemented for the unsteady terms. The *SIMPLE* algorithm is then employed to solve the discretized equations. The effect of concentration is also taken into account by

using pressure correction method to obtain the real velocity field. The averaged Sherwood and Nusselt numbers are calculated using Simpson's integration rule.

The validation procedure of the utilized method had to be done in order to check the code credibility. This is imposed as well as the convergence and grid independency tests in further steps. The time step is set close to $\Delta\tau = 0.005$ during all simulations similar to the study of Ouertatani et al. [27]. The heat and mass transfer characteristics in addition to the fluid flow patterns have been reported when the steady state conditions are achieved. The unsetady patterns of the studied thermo-solutal system are illustrated in Fig. 2, where the temporal variations of isotherm and isoconcentration contours are presented. It can be seen that after $\tau = 1000$, steady state conditions are achieved. The steady state conditions are also examined by the investigation of typical temporal variations of total kinetic energy in Fig. 3. It is observed that after an initial unsteadiness, double-diffusive convection in various regimes become as steady as the total kinetic energy attains a canstant value. The convergence of the numericall results is also employed and the following criterion is satisfied on each time step.

$$\sum_{i,j}\left|\Pi_{i,j}^{n}-\Pi_{i,j}^{n-1}\right|\leq 10^{-6}$$

Here, the generic variable Π illustrates the set of U, V, Θ, or Φ, while n represents the iteration number in each individual time step. The subscript sequence (i,j) represents the space coordinates of the grid node. The simulations were performed for three various uniform grids, *i.e.* 80×80, 90×90, and 110×110, for an especific case when $Re = 100$, and $Ri = 0.01$, and then the results were compared to gether in order to sure on grid independency. The obtained results have an excellent agreement and so, 90×90 grid was used in according to the proper accuracy as well as CPU consuming time.

considering simulated accuracy and CPU time in the range of variables adequate, results are obtained using node points 90×90.

The utilized method was validated against published results of Al-Amiri et al., [11] and Teamah & El-Maghlany [28] to sure on the accuracy of the future obtained results. Hence, numerical simulations in the absence of SD-effects, $Sr = Df = 0$, were performed for double-diffusive mixed convection flow in a vertical square enclosure with the uniformly imposed high and low temperature as well as concentration along the lower and upper walls, respectively. Fig. 4 shows the streamlines, isotherms, and isoconcentration distributions with, $Pr = 1$, $Le = 10$, $A = 1$, and $Ri = 0.01$, obtained by (a) present code, (b) Teamah & El-Maghlany [28], and (c) Al-Amiri et al. [11]. The figures show a good agreement between the results obtained by the present code and the others. Another test is conducted to check the accuracy of the utilized method, whereby the stream function values at the primary vortex location were computed for two different Reynolds number, *i.e.* 100 and 400, and are compared with the results obtained by Al-Amiri et al. [11] and Screibr & Keller [29] in Table 1. It can be seen that an excellent agreemnt was achieved between registered data results. Furtheremore, the average Nusselt number obtained by the present method and the results achieved by Sharif [30] and Malleswaran & Sivasankaran [31] are compared in Table 2. The results obtained by the present method have an acceptable aggreement with the available results, especially at the larger Re and Gr_T values.

Table 1. Comparison of primary vortex stream function.

Re	Present work	Ref. [11]	Ref. [29]
100	-0.1031	-0.1033	-0.1033
400	-0.1137	-0.1139	-0.1138

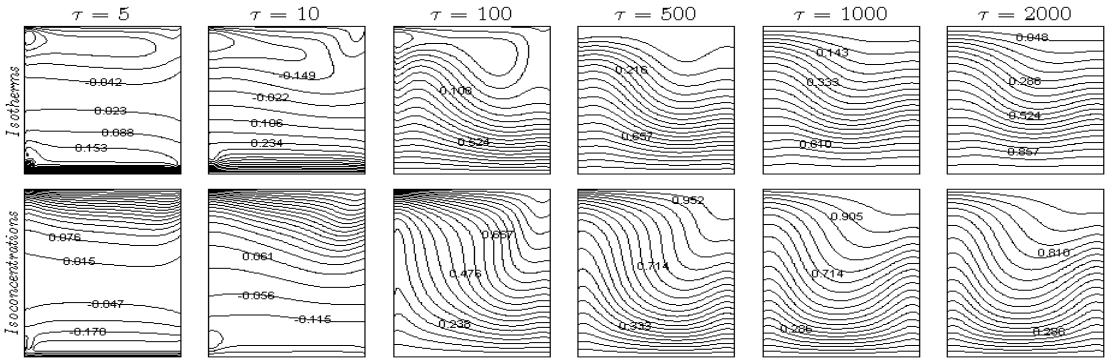

Fig. 2. Time traces of the isotherms and isoconcentrations when Ri = 10, and Sr=Df=0.25.

4. Results and Discussion

As was mentioned before, the main aim of the present work is to characterize the thermo-solutal/double-diffusive convection flow, heat and mass transfer in a square enclosure and in the presence of Soret and Dufour effects. For this purpose, numerical simulations are carried out with the validated method for different Richardson numbers ($Ri = 0.01, 0.1, 1, 10$), when Gr_T is kept constant at 10^4 and Re is varied between 31.6 to 1000. Besides, Soret and Dufour effects are employed where Sr is kept constant at 0.25, and Df is varied between 0 to 3. Schmidt number sets equal to Prandtl number, and so $Le = Sc/Pr = 1$. The assumed value of Lewis number represents a same contribution for both of heat and mass transfer, whereby it makes an upportunity to stduy the influence of Richardson number individually. Buoyancy ratio B, is also set to unity to consider similar effects for mass and thermal diffusions. Streamlines, isotherms, and isoconcentrations of the cases with different Ri and various sets of $Sr\&Df$ coefficients are displayed in Fig. 5. As can be seen that an unicellular clockwise primary vortex almost occupies whole the cavity in all the studied cases.

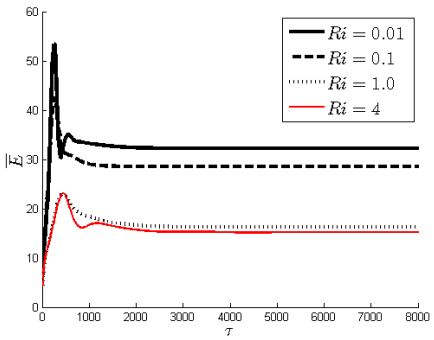

Fig. 3. Temporal variations of total kinetic energies for various Richardson numbers when $Sr = Df = 0.25$.

In fact, the fluid rises up from the heated bottom wall due to the thermal buoyancy forces and flows down along the cold side. The competition between forced flow introduced by top moving wall, solutal and thermal buoyancy forces have been formed a primary rotating cell. If the isotherm patterns of the cases with $Df = 0$ are compared together, it can be seen that the concentration of thermal boundary layers near the heated wall reduces as Richardson number enhances. To help to better understand, the isotherm patterns of the cases with $Df = 0$ are represented in Fig. 6. When Richardson number has its lowest value (Fig. 6(a)), Reynolds number is kept constant at 1000, the flow was dominated by forced convection introduced by top moving lid and the convection circulation was developed greatly. In the other words, shear forces push the convection to penetrate much deeper into the enclosure. A similar observation was reported before in the studies of Al-Amiri et al. [11], and Teamah & El-Maghlany [28], where the double diffusive mixed convection in the absence of SD-effects was investigated numerically.

However, with either decreasing Reynolds number or increasing Richardson number (Figs. 6(b)&(c)), the opposing action of thermal buoyancy forces against forced flow was pronounced, whereby the concentration of the thermal boundary layers in the vicinity of the hot wall was reduced. When $Ri = 10$ (Fig. 6(d)), the entire isotherm lines were became parallel to the horizontal walls. This configuration demonstrate that heat was transferred mostly by conduction mode, whereby the enclosure could be assumed as a quasi-conduction domain. It should be noted that the isotherm and isoconcentration patterns in the cases with $Df = 0$ are almost similar due to the value of Lewis number, *i.e.* $Le = 1$. This fact is not repeated when either the extra mass or thermal diffusion is introduced.

Table 2. Comparison of the average Nusselt numbers.

		Average Nusselt number		
Re	Gr	Present study	Ref. [30]	Ref. [31]
400	10^2	3.94	4.05	4.08
	10^4	3.72	3.82	3.84
	10^6	1.22	1.17	1.10
1000	10^2	6.35	6.55	6.48
	10^4	6.31	6.50	6.47
	10^6	1.78	1.81	1.66

Fig. 5 also depicts that at the lower and moderate values of Dufour coefficient, *i.e.* $Df = 0.25$ and 1, the influence of SD-effects on fluid flow, isotherms, and isoconcentrations seems to be insignificant. In addition, the influence of SD-effects on even fluid flow can be ignored when Richardson number is large enough. Nevertheless, Figs. 5(c)&(d) show that the enhancement of Dufour coefficient could develop fluid flow and transport phenomena when flow is in the mixed or natural convection regime. The extra thermal diffusion within the enclosure, which was increased by increasing Dufour coefficient, is in the direction of concentration gradient, and so has an aiding and opposing action on the shear forces and thermal buoyancy forces, respectively. As it was mentioned earlier, the shear forces introduced by top moving wall, have a tendency to push the convection into the enclosure, whereby the thermal boundary layers are concentrated greatly near the hot wall with further decreasing of Richardson number. Therefore, the competition between forced convection on one side and thermal buoyancy forces as well as extra thermal diffusion introduced by SD-effects on the other side, forms thermal eddies near the heated wall. Those thermal eddies cause a distortion in the thermal boundary layers even if when the enclosure is a quasi-conductive domain. In addition, the extra thermal diffusion disturbs the equilibrium between mass and thermal diffusing, assumed before by implying $Le = 1$, and so isotherms and isoconcentrations are not the same here.

Figs. 5(c)&(d) represents that when Richardson number was increased and so forced convection was ground by natural flow, the extra thermal diffusion along with the thermal buoyancy forces have formed the secondary eddies at the left bottom of the enclosure. It can be seen that the secondary eddy formation is augmented with increasing either Richardson number or Dufour coefficient. On the other hand, it seems that the variation of Dufour coefficient was also affected to some extent on the isoconcentration contours. This is attributed to the fact that the mass transfer rate was affected to some extent by convection activities.

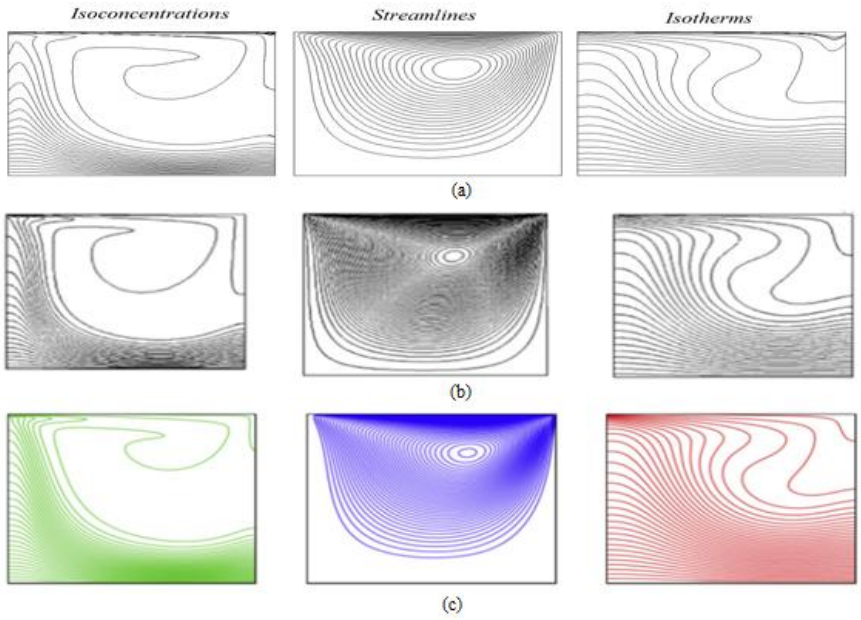

Fig. 4. Streamlines, isotherms, and isoconcentrations for Pr = 1, Le = 10, A = 1, and Ri = 0.01, obtained by (a) present method, (b) Teamah & El-Maghlany [28], and (c) Al-Amiri et al. [11].

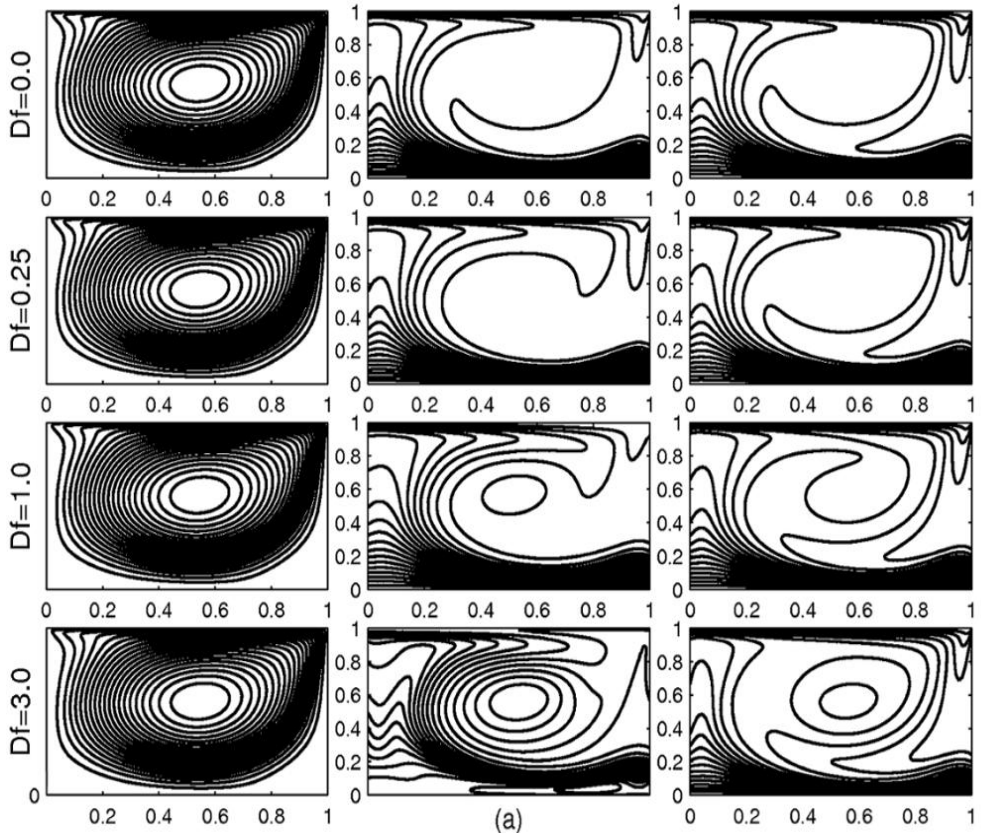
Df=0.0
Df=0.25
Df=1.0
Df=3.0
0 0.2 0.4 0.6 0.8 1

(a)

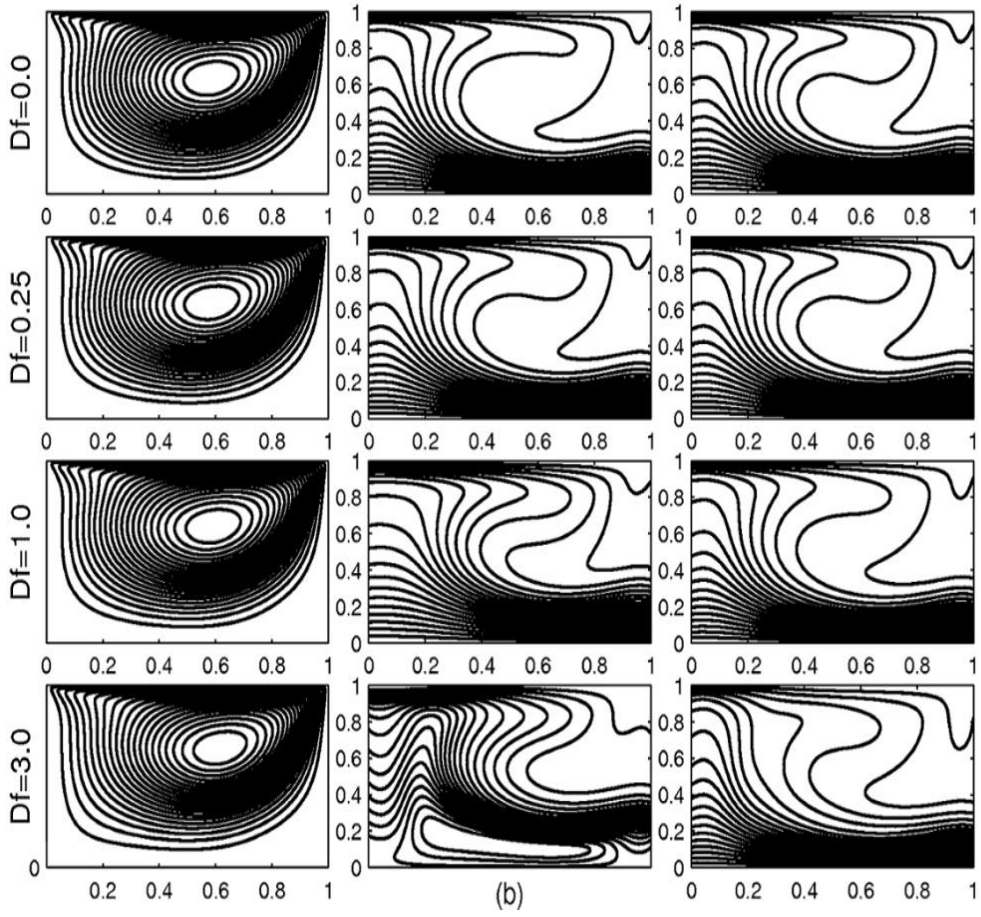
Df=0.0
Df=0.25
Df=1.0
Df=3.0
0 0.2 0.4 0.6 0.8 1

(b)

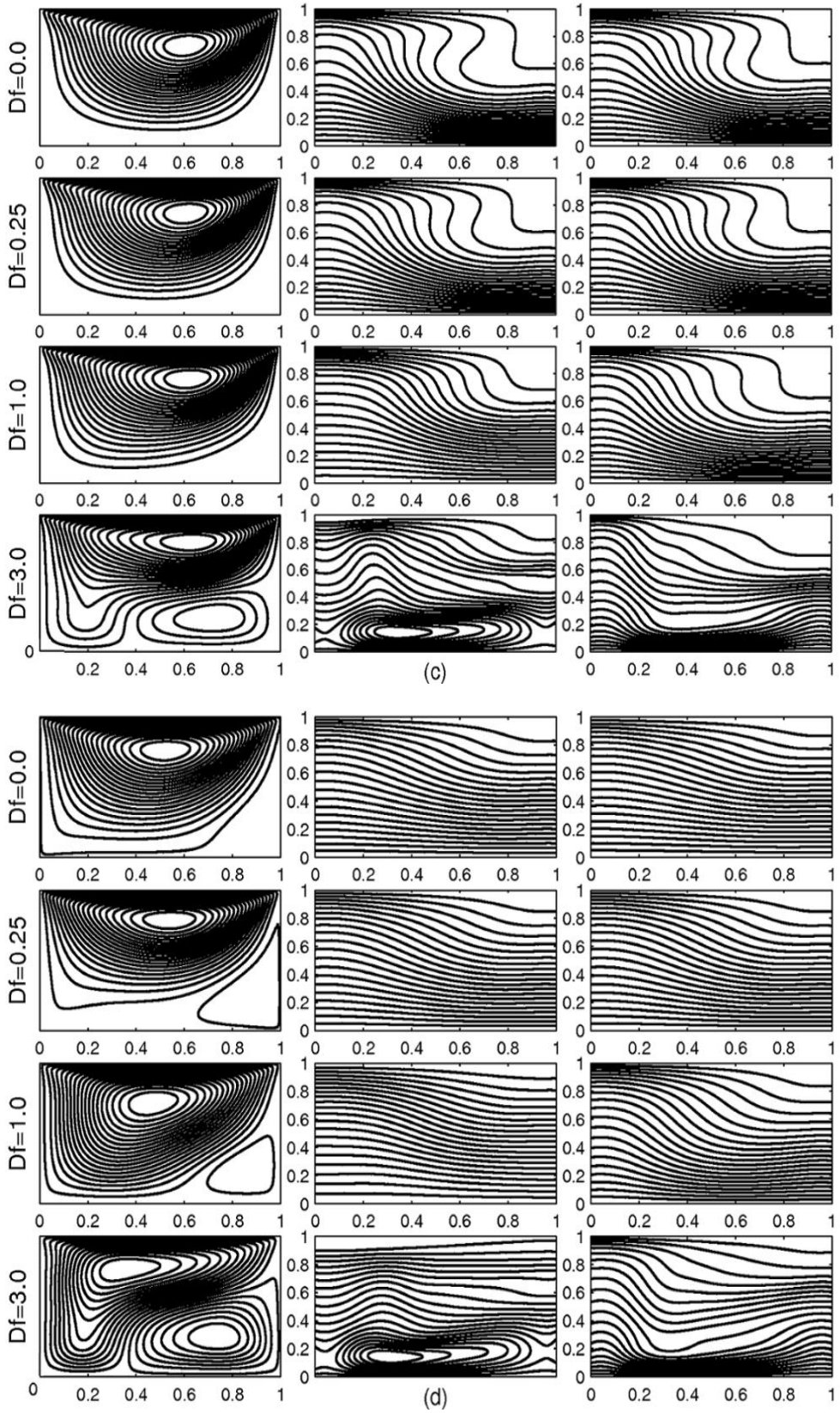

Fig. 5: Streamlines (left column), isotherms (middle column), and isoconcentrations (right column) for (a) $Ri = 0.01$, (b) $Ri = 0.1$, (c) $Ri = 1$, and (d) $Ri = 10$, when $Sr = 0.25$ and $Gr_T = 10^4$.

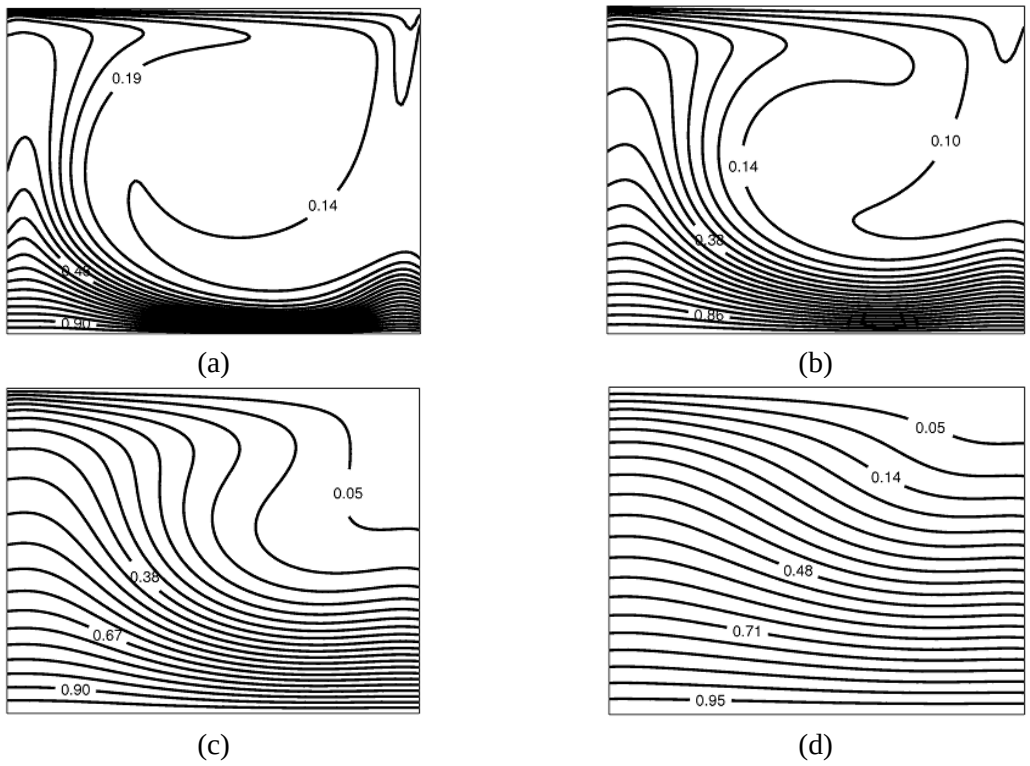

Fig. 6: Isotherm patterns for (a) $Ri = 0.01$, (b) $Ri = 0.1$, (c) $Ri = 1$, and (d) $Ri = 10$, when $Df = 0$ and $Sr = 0.25$.

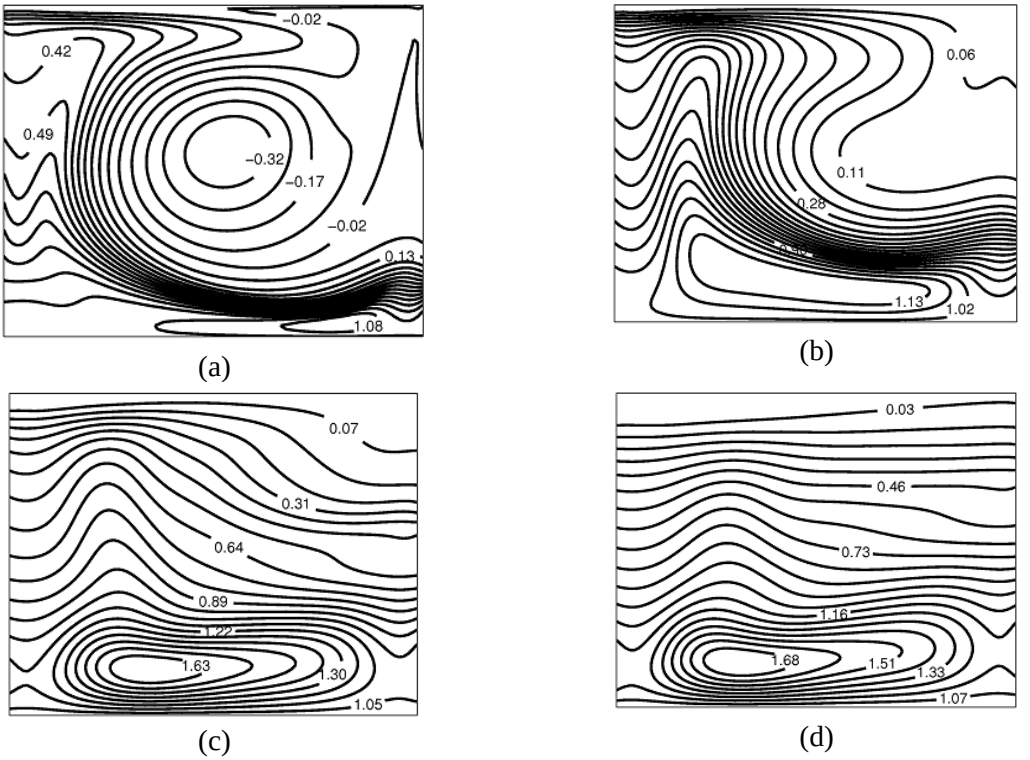

Fig. 7: Isotherm patterns for (a) $Ri = 0.01$, (b) $Ri = 0.1$, (c) $Ri = 1$, and (d) $Ri = 10$, when $Df = 3$ and $Sr = 0.25$.

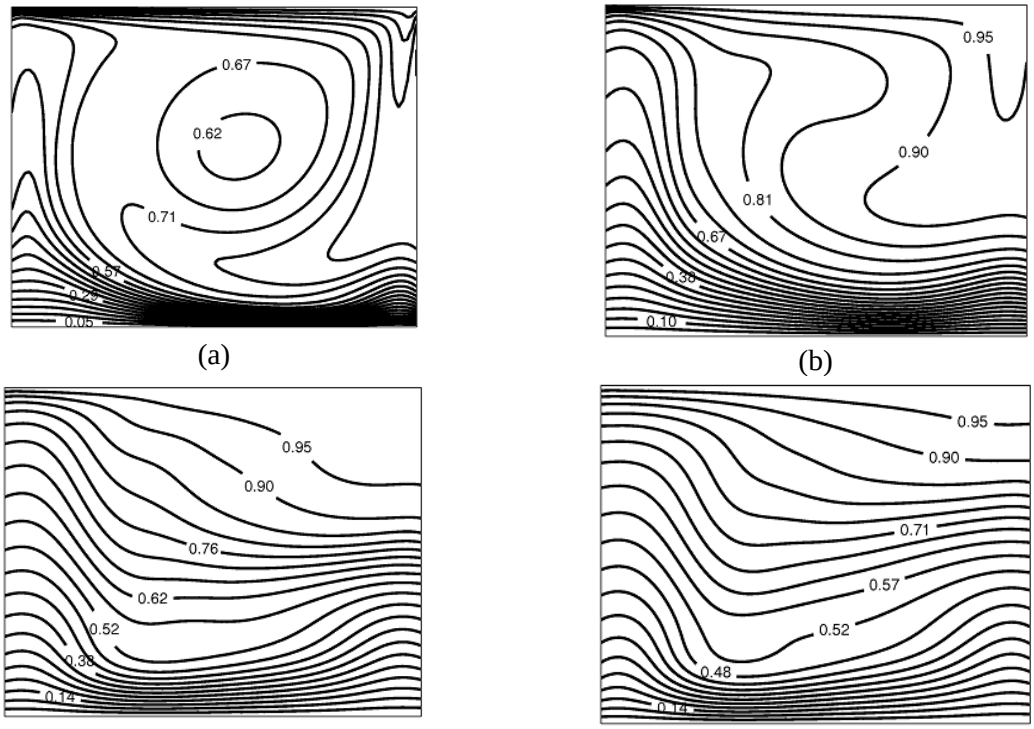

Fig. 8: Isoconcentration patterns for (a) $Ri = 0.01$, (b) $Ri = 0.1$, (c) $Ri = 1$, and (d) $Ri = 10$, when $Df = 3$ and $Sr = 0.25$.

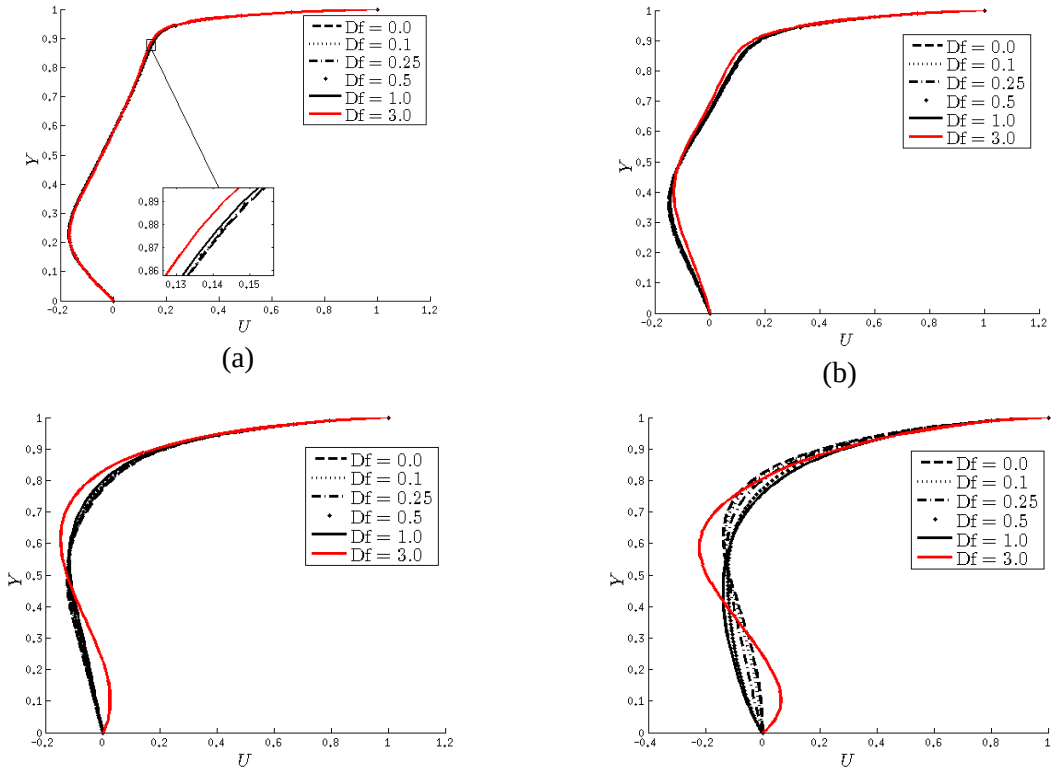

Fig. 9: Horizontal mid-velocity profiles for (a) $Ri = 0.01$, (b) $Ri = 0.1$, (c) $Ri = 1$, and (d) $Ri = 10$. In all of cases $Sr = 0.25$.

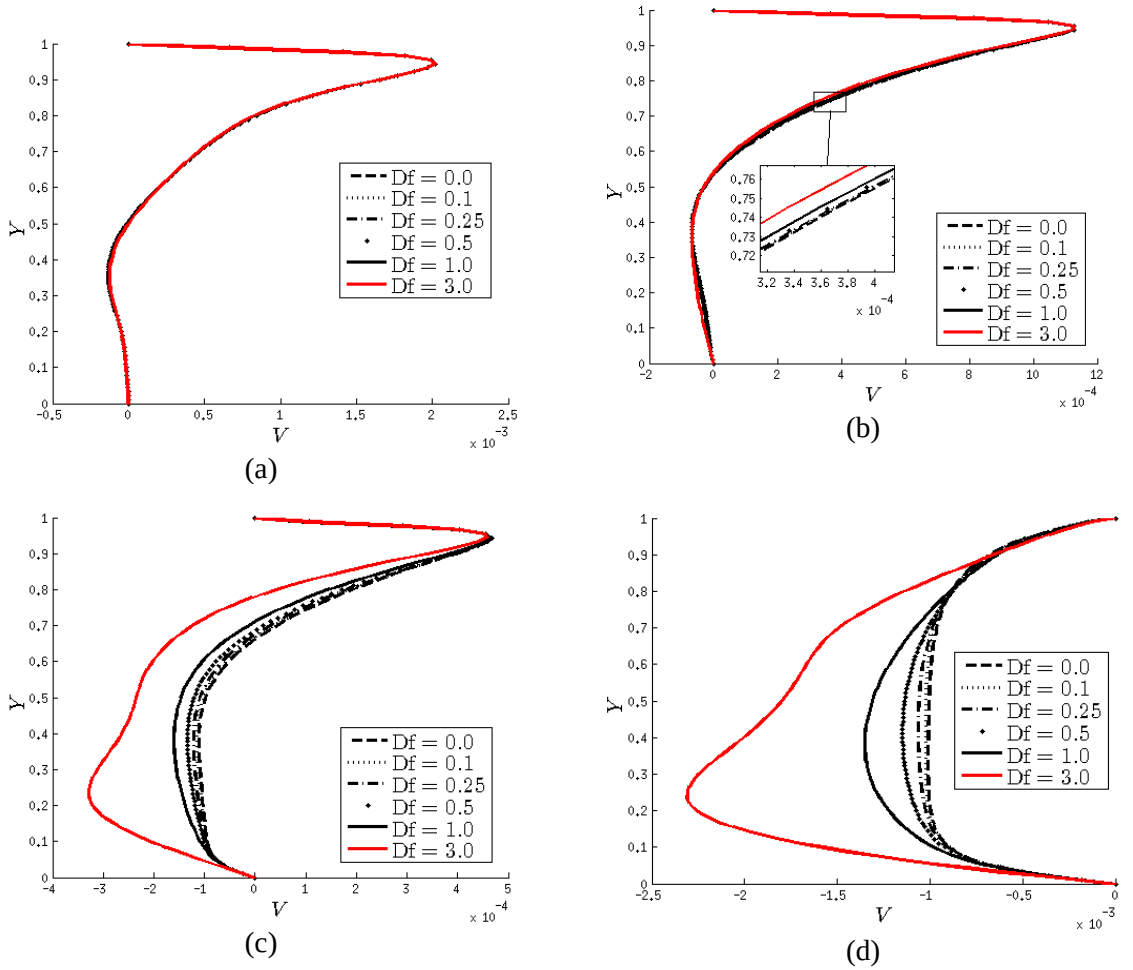

Fig. 10: Vertical mid-velocity profiles for (a) $Ri = 0.01$, (b) $Ri = 0.1$, (c) $Ri = 1$, and (d) $Ri = 10$. In all of cases $Sr = 0.25$.

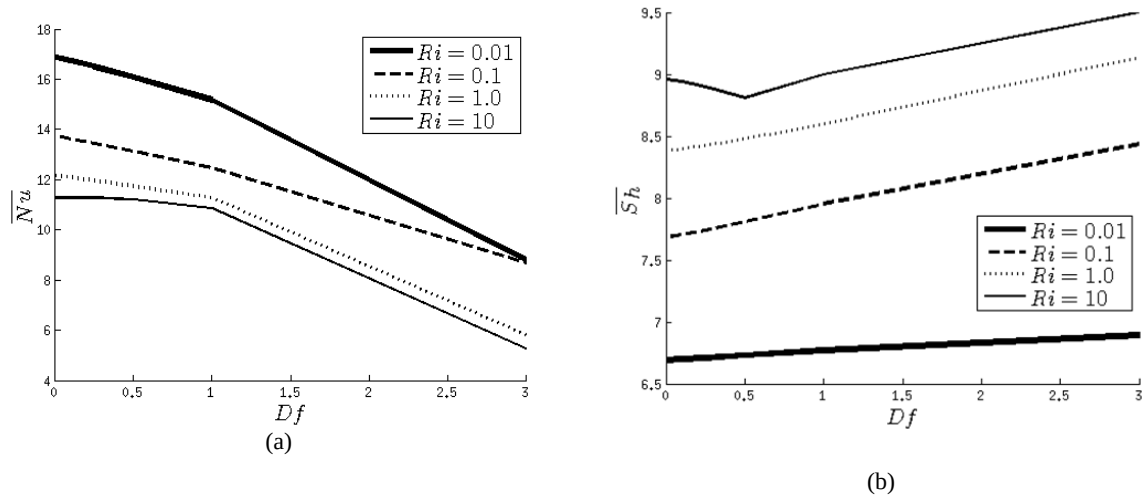

Fig. 11: Average (a) Nusselt, and (b) Sherwood numbers, when $Sr = 0.25$ for all cases.

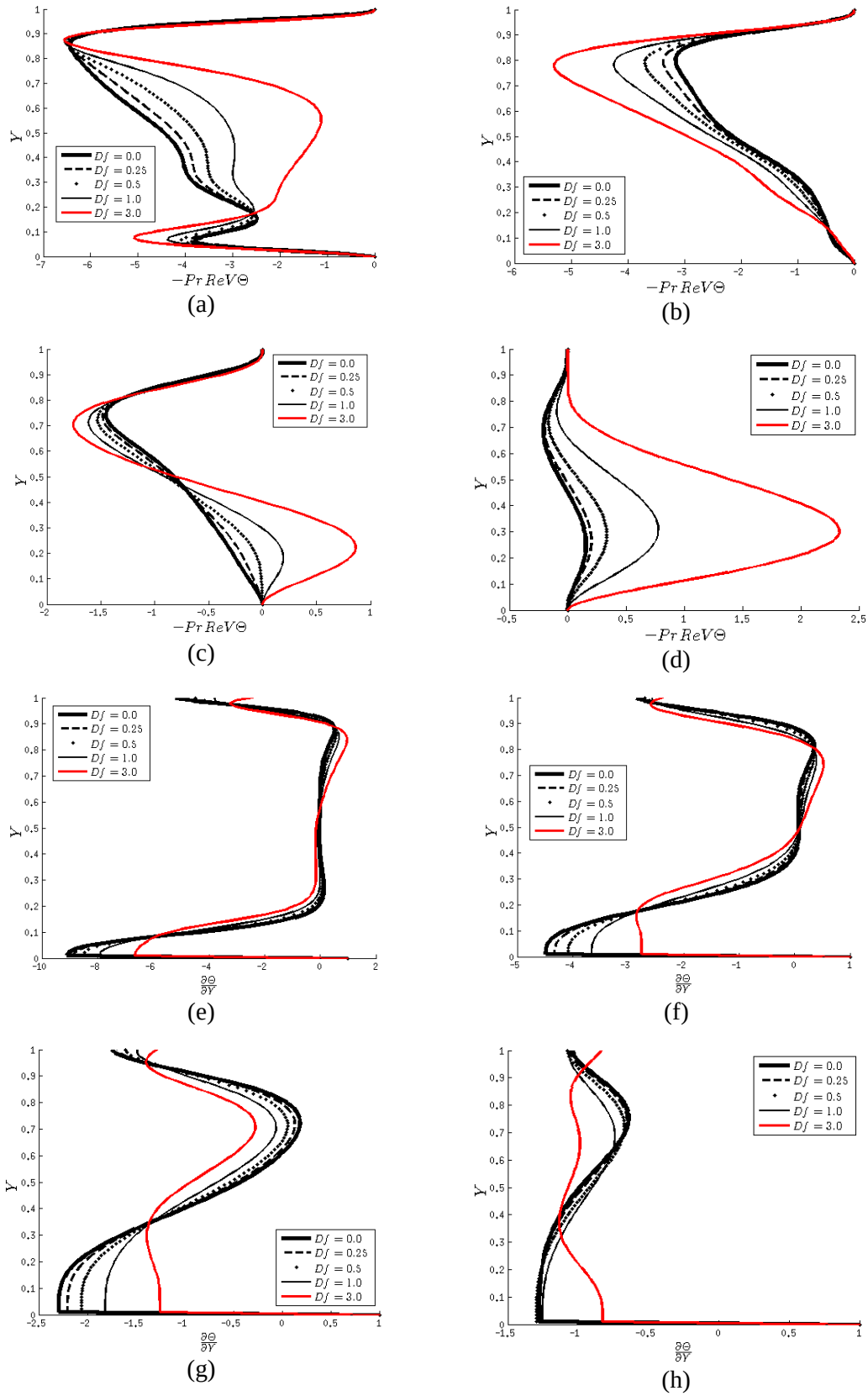

Fig. 12: The vertical distributions of conduction mode of heat transfer along the mid-plane of the square enclosure for (a) $Ri = 0.01$, (b) $Ri = 0.1$, (c) $Ri = 1$, and (d) $Ri = 10$, and the vertical distributions of convection mode of heat transfer along the mid-plane of the square enclosure for (a) $Ri = 0.01$, (b) $Ri = 0.1$, (c) $Ri = 1$, and (d) $Ri = 10$, where $Sr = 0.25$ in all of cases

To better examine the behavior of transport phenomena in the presence of SD-effects, the isotherm and isoconcentration patterns for the cases with largest Df value ($Df = 3$) are represented in Figs. 7&8, respectively. Figs. 7(a)-(d) show that the thermal boundary layers form upper than the bottom heated wall, whereby the thermal eddies separate those boundary layers from the wall. It can also be seen that the intensity of those thermal eddies was augmented by increasing Richardson number. In other words, the thermal eddies due to the extra thermal diffusion were intensified when flow was dominated by natural convection. On the other hand, the value of isotherm lines increases as Richardson number enhances. This fact show that temperature gradient within the cavity increases as the Richardson number enhances. Meanwhile, the negative value of isotherm line represents the loss of buoyancy forces across the enclosure. Figs. 8(a)-(d) depict that isoconcentration patterns were affected by Richardson number variation when Dufour coefficient is a large value, *i.e.* $Df \geq 1$. This feature may be due to the non-zero value of the Soret coefficient. As was observed before in Figs. 7(a)-(d), the temperature gradient across the enclosure enhances with increasing Richardson number and Dufour coefficient simultaneously. The large temperature gradient in according to the non-zero value of Soret coefficient produces extra mass diffusion which affects to some extent on isoconcentration patterns.

The horizontal and vertical velocity profiles along the mid-plane of the enclosure are displayed in Figs. 9&10, respectively. As can be seen that when$Ri < 1$, the influence of SD-effects on velocity profiles seems to be insignificant in spite of some observed minor deviations. This fact again demonstrates that the influence of SD-effects on fluid characteristics can be ignored when flow was dominated by forced convection. In addition, Figs. 9(b)-(d) show that the cases with largest Dufour coefficient have largest horizontal velocity components near the heated wall. This feature was also pronounced with increasing Richardson number. The formation of thermal eddies in cases with largest Dufour coefficient which was explained before can be recognized as the main reason of this feature. However, it was denoted earlier that the Dufour effect has an opposite effect on the thermal buoyancy forces provoked by the heated wall. This fact is observed again in Figs. 10(a)&(b), whereby the vertical component of the velocity at the bottom half of the enclosure was reduced by increasing Dufour coefficient. In order to assess the convective heat and mass transfer within the enclosure, the variations of the average Nusselt and Sherwood numbers as a function of Dufour coefficient for all of the studied cases are elucidated in Fig. 11. The joint effect of varying Ri and Df upon the heat and mass transfer processes is undoubtedly noticeable in these plots. Fig. 11(a) shows that the average Nusselt number variations are in good agreement with isotherm plots, previously commented. For instance, for either larger Richardson number or smaller Dufour coefficients, the average Nusselt numbers are small to some extent. This fact represents that the conduction is the dominant mechanism of transport phenomena here. Furthermore, Fig. 11(b) shows that the average Sherwood number was enhanced with increasing either Dufour coefficient or Richardson number. In according to the non-zero value of Soret coefficient and implemented boundary conditions, it seems that the augmentation of temperature gradient caused by increasing either heat diffusion or thermal buoyancy forces, causes an enhancement in mass transfer through the enclosure. The influence of pertinent parameters on the various heat transfer modes are illustrated in Fig. 12. In particular, Figs. 12(a)-(d) show the variations of convective mode of heat transfer within the enclosure. First, it can be observed that the convective mode of heat transfer at the bottom half of the enclosure and especially in the vicinity of the heated wall was augmented by further increasing of Richardson number, whereby the bottom peak of the figures was moved from the negative side towards the positive side with an enhancement of Ri value. When $Ri = 0.01$, the aiding action of Dufour effect against the shear forces, increases convective mode of heat transfer at the core of the enclosure. In contrast, the opposite action of the extra heat diffusion against the thermal buoyancy forces reduces the convective mode of heat transfer near the heated wall. With an enhancement of Richardson number, the influence of thermal buoyancy forces was expanded from near the heated wall towards the core of the enclosure. This fact causes that the competition of Dufour effect and thermal buoyancy forces moves towards the upper half of the enclosure. With further increasing of Richardson number and when flow was dominated by natural convection, the extra heat diffusion has an aiding effect on the convection recirculation of the enclosure, whereby the convective mode of heat transfer at the core of the

cavity was improved when Dufour coefficient enhances.

The effect of pertinent parameters on the conductive mode of heat transfer is shown in Figs. 12(e)-(h). In here, the variation of the normal temperature variations along the vertical mid-plane of the enclosure is illustrated. When Ri was decreased to 0.01, the forced convection invigorates and heat transfer penetrates much deeper into the enclosure. This fact causes that the conductive mode of heat transfer in forced convection regime is submerged at the core of the enclosure and tended towards a zero value. However, it can be seen that the absolute value of the normal temperature variations near the heated wall was enhanced by decreasing Richardson number. This fact represents the concentrated thermal boundary layers in that region which observed before in Fig. 5. In addition, the extra heat diffusion has an opposing action with respect to the conductive mode of heat transfer near the heated wall. The thermal eddies which was formed by increasing Dufour coefficient, observed before in Fig. 7, can be recognized as the main reason of the behaviour of conductive mode of heat transfer near the heated wall.

This work is wrapped by the investigation of the total kinetic energy variation across the enclosure. To help to better understand, the cases with $Ri = 4$ were just added here. The variation of average total kinetic energy as a function of Dufour coefficient for various convection regimes is represented in Fig. 13. It can be observed that $\bar{E}$ was increased with reducing Richardson number when the influence of the extra heat diffusion was ignored, $Df = 0$. However, the variations of total kinetic energy as a function of Dufour coefficient manifests variety fashions depends mainly on the Richardson number value. In moderate and small Richardson numbers, it was reduced with increasing of the Dufour coefficient, while the opposite was achieved for the cases with $Ri > 1$. This can be due to the influence of Dufour coefficient on the convective mode of heat transfer observed before in Fig. 12. In other words, increasing the convective mode of heat transfer would improve total kinetic energy of the enclosure.

In further, a quadratic curve fitting of the average total kinetic energy with Dufour coefficient is implemented [32]. The fitted model is the form:

$$\bar{E} = aDf^2 + bDf + c \quad (16)$$

The values of coefficients a, b, and c with standard error of quadratic curve fitting for various Richardson numbers are calculated and registered in Table 3.

In addition a linear curve fitting was also utilized on a, b, and c coefficients and Richardson number, whereby the following relation is obtained for total kinetic energy as follows:

$$\bar{E} = (-0.24Ri + 0.3)Df^2 + (0.9Ri - 0.7)Df + 0.2Ri + 24.7 \quad (17)$$

The variations of total kinetic energy obtained by the relation above and data results achieved by numerical method are compared in Fig. 14. An acceptable agreement is observed between the obtained results. Therefore, Eq. (17) can well be utilized for estimating the average total kinetic energy of double-diffusive mixed convection in presence of Dufour effect.

Table 3. The coeffiecients and standard errors of quadratic curve fitting of total kinetic energy.

Ri	a	b	c	Standard Error
0.01	-0.0047	-0.0853	24.926	0.0002
0.1	0.0061	0.54	24.76	0.0008
1	0.093	-1.4076	24.513	0.0012
4	-2.2136	4.0211	23.339	0.0072
10	-2.3423	7.9829	22.728	0.0081

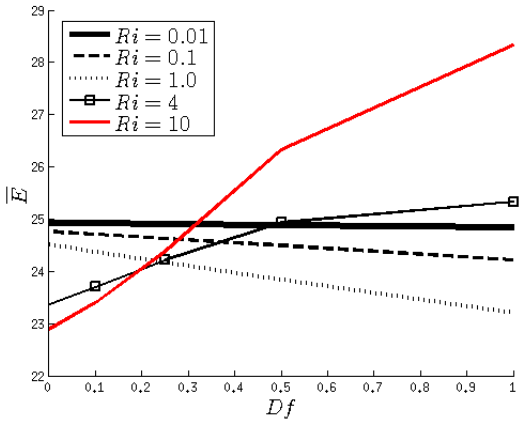

Fig. 13. The average total kinetic energy versus Dufour coefficient for diferent Richardson numbers

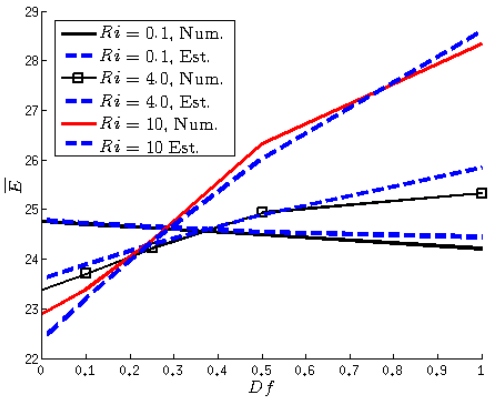

Fig. 14. The comparison of obtained results by numerical method (Num.) and estimated by Eq. (17) (Est.).

5. Conclusions

The present work addressed a numerical characterization of thermo-solutal mixed convection in a lid-driven square enclosure and in the presence of extra mass and energy diffusions named Soret and Dufour effects. The effects of varying Richardson number as well as Soret and Dufour coefficients on the resulting thermo-solutal convection are examined and investigated. In addition, the influence of those pertinent parameters on the heat and mass transfer, various modes of heat transfer, and total kinetic energy of the thermo-solutal system are evaluated and discussed in detail. The main conclusions earned from this study are listed below:

1. The influence of Soret and Dufour effects on fluid flow and transport phenomena seems to be insignificant when flow is dominated by forced convection.
2. Thermal eddies formed by the competition of extra heat diffusion and thermal buoyancy forces at the bottom half of the enclosure causes a reduction in the natural convection heat transfer.
3. The average Nusselt number decreases as Dufour coefficient and/or Richardson number increases.
4. The average Sherwood number increases as Dufour coefficient and Richardson number enhance. It seems that the extra heat diffusion has an aiding effect on convective current of mass across the cavity.
5. Dufour effect has an opposing action against the conductive mode of heat transfer especially at the vicinity of the hot wall.
6. The enhancement of convective heat transfer within the enclosure causes an improvement in the total kinetic energy of the thermo-solutal system.

Acknowledgements

The author wish to aknowledge anonymous reviwers whose constructive comments improved the presentaion of this work.

Nomenclature

B	buoyancy ratio
C	concentration (kgm^{-3})
C_0	characteristic concentration
D_m	diffusion coefficient (m^2s^{-1})
Df	dimensionless Dufour coefficient
g	gravity acceleration (ms^{-2})
Gr_C	solutal Grashof number
Gr_T	thermal Grashof number
L	enclosure with (m)
Le	Lewis number
Nu	Nusselt number
p	fluid pressure (Nm^{-2})
Pr	Prandtl number
Re	Reynolds number
Ri	Richardson number
Sc	Schmidt number
Sh	Sherwood number
Sr	dimensionless Soret coefficient
T	fluid temperature (K)
T_0	characteristic fluid temperature
U_0	absolute lid velocity (ms^{-1})

Greek

α_m	thermal diffusivity (m^2s)
β_C	concentration expansion coefficient (K^{-1})
β_T	thermal expansion coefficient (K^{-1})
κ_{CT}	Soret coefficient ($m^{-1}K^{-1}kgs^{-1}$)
κ_{TC}	Dufour coefficient (m^5Kkgs^{-1})

ν	kinematic viscosity of fluid (m^2s^{-1})
Φ	dimensionless concentration
ψ	stream function
ρ	fluid density (kgm^{-3})
ρ_0	characteristic fluid density
Θ	dimensionless temperature
subscript	
h	high
l	low

References

[1]. R.W. Schmit, "Double diffusion in oceanography," Annual Review of Fluid Mech, 26, 255–265, (1994).

[2]. R.El. Ayachi, A. Raji, M. Hasnaoui, A. Abdelbaki, M. Nami, "Resonance of double-diffusive convection in a porous medium heated with a sinusoidal exciting temperature," Journal of. Applied Fluid Mechanica, 3, 43–52, (2010).

[3]. P.K. Bose, D. Sen, R. Panua, A.K. Das, "Numerical analysis of laminar natural convection in a quadrantal cavity with a solid adiabatic fin attached to the hot vertical wall. Journal of. Applied Fluid Mechanica, 6, 501-510, (2013).

[4]. A.A. Abbasian Arani, M. Mahmoodi, S. Mazrouei Sebdani, "On the cooling process of nanofluid in a square enclosure with linear temperature distribution on left wall," Journal of. Applied Fluid Mechanica, 7, 591-601, (2014).

[5]. J.Serrano-Arellano, J. Xama`n, G. A`lvarez, "Optimum ventilation based on the ventilation effectiveness for temperature and CO_2 distribution in ventilated cavities," International Journal of Heat and Mass Transfer, 62, 9–21, (2013).

[6]. S. Bettaibi, F., Kuznik, E. Sediki, "Hybrid LBM-MRT model coupled with finite difference method for double-diffusive mixed convection in rectangular enclosure with insulated moving lid," Physica A: Statistical Mechanics and its Applications, 444, 311-326, (2016).

[7]. A.M. Aly, "Double-diffusive natural convection in an enclosure including/excluding sloshing rod using a stabilized ISPH method," International Communications in Heat and Mass Transfer, 73, 84-99, (2016).

[8]. J.W. Lee, J.M. Hyun, "Double-diffusive convection in a rectangle with opposing horizontal temperature and concentration gradients," International Journal of Heat and Mass Transfer, 32, 1619–1632, (1990).

[9]. J.M. Hyun , J.W. Lee, "Double-diffusive convection in a rectangle with cooperating horizontal gradients of temperature and concentration," International Journal of Heat and Mass Transfer, 32, 1605–1617, (1990).

[10]. H.F. Oztop, I. Dagtekin, "Mixed convection in two-sided lid-driven differentially heated square cavity," International Journal of Heat and Mass Transfer, 47, 1761–1769, (2004).

[11]. A. Al-Amiri, K. Khanafer, K., J. Bull, I. Pop, "Numerical simulation of combined thermal and mass transport in a square lid-driven cavity," International Journal of Thermal Science 46, 662–671, (2007).

[12]. Q. Qin, Z.A. Xia, Zhen F. Tian, "High accuracy numerical investigation of double diffusive convection in a rectangular enclosure with horizontal temperature and concentration gradients," International Journal of Heat and Mass Transfer, 71, 405–423, (2014).

[13]. Sofen K. Jena, Laxman K. Malla, Swarup K. Mahapatra, Ali J. Chamkha, "Transient buoyancy-opposed double diffusive convection of micropolar fluids in a square enclosure," International Journal of Heat and Mass Transfer 81, 681–694, (2015).

[14]. P. Bhattacharya, S. Das, "Study on steady natural convective heat transfer inside a square cavity for different values of Rayleigh and Nusselt numbers. Journal of Applied Fluid Mechanics 8, 635–640, (2015).

[15]. L. Wang, B. Shi, Z. Chai, X. Yang, "Regularized lattice Boltzmann model for double-diffusive convection in vertical enclosures with heating and salting from below," Applied Thermal Engineering, 103, 365–376, (2016).

[16]. M.S. Malashetty, S.N., Gaikwad, "Effect of cross diffusion on the onset of double diffusive convection in a porous medium," International

Applied Mechanical Engineering, 6, 675–691, (2001).

[17]. L.K. Rebi, A. Mojtabi, M.J. Safi, A.A. Mohammad, "Numerical study of thermo-solutal convection with Soret effect in a square cavity," International Journal of Heat and Fluid Flow 18, 561–579, (2008).

[18]. M. Bhuvaneswari, S. Sivasankaran, Y.J. Kim, "Numerical study on double-diffusive mixed convection with a Soret effect in a two-sided lid-driven cavity," Numerical Heat Transfer A, 59, 543–560, (2011).

[19]. J. Wang, M. Yang, Y. Zhang, "Onset of double-diffusive convection in horizontal cavity with Soret and Dufour effects," International Journal of Heat and Mass Transfer, 78, 1023–1031, (2014).

[20]. Q. Ren, C.L. Chan, "Numerical study of double-diffusive convection in a vertical cavity with Soret and Dufour effects by lattice Boltzmann method on GPU," International Journal of Heat and Mass Transfer, 93, 538–553, (2016).

[21]. Gh.R. Kefayati, "Simulation of double diffusive natural convection and entropy generation of power-law fluids in an inclined porous cavity with Soret and Dufour effects (Part I: Study of fluid flow, heat and mass transfer)," International Journal of Heat and Mass Transfer, 94, 539–581, (2016).

[22]. J. Wang, M. Yang, Y-L He, Y. Zhang, "Oscillatory double-diffusive convection in a horizontal cavity with Soret and Dufour effects," International Journal of Thermal Sciences, 106, 57–69, (2016).

[23]. A. Barletta, E. Zanchini, "On the choice of the reference temperature for fully developed mixed convection in a verticle channel," International Journal of Heat and Mass Transfer, 42, 3169–3181, (1999).

[24]. T. S. Cheng, "Characteristics of mixed convection heat transfer in a lid-driven square cavity with various Richardson and Prandtl numbers," International Journal of Thermal Science, 50, 197–205, (2008).

[25]. O. Goyan, "High-Reynolds number solutions of Navier-Stokes equations using incremental unknowns," Computational Methods in Applied Mechanical Engineering, 130, 319-335, (1996).

[26]. S.V. Patankar, "Numerical heat transfer and fluid flow," Hemisphere, Washington D.C. (1980).

[27]. N. Ouertatani, N.B. Cheikh, B.B. Beya, T. Lili, A. Campo, "Mixed convection in a double lid-driven cubic cavity," International Journal of Thermal Science, 48, 1265–1272, (2009).

[28]. M.A. Teamah, W.M. El-Maghlany, "Numerical simulation of double-diffusive mixed convection in rectangular enclosure with insulated moving lid," International Journal of Thermal Science, 49, 1625–1638, (2010).

[29]. R. Screiber, H.B. Keller, "Driven cavity flows by efficient numerical techniques," Journal of Computational Physics 49, 310–333, (1983).

[30]. M.A.R. Sharif, "Laminar mixed convection in shallow inclined driven cavities with hot moving lid on top and cooled from bottom," Applied Thermal Engineering 27, (2007), 1036–1042, (2007).

[31]. A. Malleswaran, S. Sivasankaran, "A numerical simulation on MHD mixed convection in a lid-driven cavity with corner heaters," Journal of Applied Fluid Mechanics, 9, 311-319, (2016).

[32]. T. R. Mahapatra, D. Pal, S. Mondal, "Effects of buoyancy ratio on double-diffusive natural convection in a lid-driven cavity," International Journal of Heat and Mass Transfer, 57, 771-785, (2013).